



Inspiring Excellence

# Study of LSPR Characteristics of Nano Bi-pyramid as metals, transition metal nitrides and transparent conducting oxides for Bio-molecule Detection

Submitted by

**Md. Hasinur Rashid -13121094**

**Syed Sanjid Ahmed -12221059**

**Kazi Miraz Al Haider-13321001**

Thesis Submitted To

The Department of Electrical and Electronics Engineering of  
BRAC University  
in Partial Fulfillment of Bachelor of Science Degree

Thesis Supervised By

**Avijit Das**

## LETTER OF TRANSMITTAL

20<sup>th</sup> August 2017

To,

Avijit Das

Department of Electrical and Electronics Engineering

BRAC University

**Subject:** Submission of thesis report for completing our graduation.

Dear Sir,

With high reverence we want to state that we have finished our thesis report on the “Analysis of LSPR Characteristics of Nano Bi-pyramid for Bio Molecule Detection”. We did some elaborate research to compile our report in a comprehensive manner. In this thesis, all the team members contributed equally with sheer hard work. We faced some challenges in working as a team and to put people’s perception. We will like to take this platform to thank you.

To end, we would like you to kindly accept our thesis report and to acknowledge our devotion and efforts.

Thanking you in anticipation.

Yours Sincerely,

MD. Hasinur Rashid

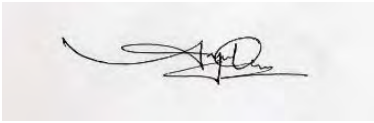
Syed Sanjid Ahmed

Kazi Miraz Al Haider

## **Declaration of Authorship**

We hereby certify that this thesis has been composed by us and is based on our own work, unless stated otherwise. Materials that support our work by other researchers are mentioned in the reference section. No other person's work has been used without due acknowledgement in this thesis. All references and verbatim extracts have been quoted, and all sources of information, including graphs and data sets, have been specifically acknowledged.

**Signature of the Supervisor:**



---

Avijit Das

**Signature of authors:**

---

Md. Hasinur Rashid

---

Syed Sanjid Ahmed

---

Kazi Miraz Al  
Haider

## **Acknowledgement**

First and foremost, we would like to express deepest gratitude to Almighty, for blessing us with the knowledge and ability to successfully complete our work in time. We want to pay our most profound appreciation to our Supervisor, **Avijit Das** for giving us the opportunity to deal with this venture under his watch. The necessary instructions and materials provided by him literally helped us to understand our topic better and analyze it effectively. Without his keen supervision, it would have been impossible for us to finish this report. Last but not the least, we would like to say thanks to our parents for their constant support and always believing in us.

## **ABSTRACT:**

The Localized Surface Plasmon Resonance (LSPR) occurs when the electrons in the nanoparticles interact with incident electromagnetic field. The potential to develop highly sensitive and specific sensors for biological targets using LSPR motivates a portion of the research in this field as we have seen the use of LSPR spectroscopy in medical diagnostics and other applications in optics, photocatalysis, medicine and photovoltaics. Extensive works have been done by various researchers on LSPR characteristics and applications largely based on Gold (Au) and Silver (Ag) nanoparticles of different structures and shapes. In our research we studied LSPR characteristics of a single nano bi-pyramid made of different materials other than gold and silver. We calculate individual material performance of nano bi-pyramid of different dimensions and background environment using Mie calculation by finding extinction and electric field intensity and create database for the purpose of bio-molecule detection.

# Table of contents

<b>Declaration of Authorship</b>	<b>ii</b>
<b>Acknowledgement</b>	<b>iii</b>
<b>Abstract</b>	<b>iv</b>
<b><u>1 Introduction</u></b>	
1.1 Localized surface Plasmon Resonance.....	1
1.2 Impacts and Applications.....	1
1.3 Motivation.....	3
1.4 Problems.....	4
1.5 Thesis Overview.....	5
<b><u>2 Theoretical background of LSPR</u></b>	
2.1 LSPR Theory.....	6
2.2 Drude Model.....	8
2.3 Mie Theory.....	10
2.4 Gans Theory.....	12
2.5 Summary.....	14
<b><u>3 Structure Design and Analysis</u></b>	
3.1 Introduction.....	15
3.2 Proposed Structure.....	16
3.3 Protein as a Biomolecule.....	17
3.3.1 Lysozyme (Lys).....	19
3.3.2 Human serum albumin (HSA).....	20
3.3.3 Human immunoglobulin (IgG).....	21
3.3.4 Human fibrinogen (Fb).....	22
3.4 Summary.....	23

<b>4</b>	<b><u>FDTD Simulation</u></b>	
4.1	Introduction .....	24
4.2	Material Modeling .....	25
4.3	Biomolecule Modeling .....	25
4.4	Mesh varying Test .....	26
4.5	Boundary Conditions .....	27
	4.5.1 Perfectly Matched Layers .....	27
	4.5.2 Symmetric/Anti symmetric .....	28
4.6	Optical Sources .....	29
4.7	Power Absorption and scattering .....	31
4.8	Summary .....	32
<b>5</b>	<b><u>Simulation and Result Analysis</u></b>	
5.1	Introduction .....	33
5.2	Aspect Ratio.....	34
5.3	Noble Metals .....	36
5.4	Conventional Metals .....	38
5.5	Transitional Metal Nitrides .....	40
5.6	Transparent Conducing Oxides .....	42
5.7	Sensitivity Analysis and FOM.....	44
5.8	Summary.....	46
<b>6</b>	<b><u>Conclusion and Future Works</u></b>	<b>47</b>
	<b><u>Bibliography</u></b>	<b>48</b>

# List of Figures

2.1	Illustration of the excitation of localized surface plasmon resonance [8] .....	6
2.2	Lycurgus cup, a piece of Ancient Roman Nanotechnology [10]. .....	7
2.3	Schematics illustration of scattering and absorption spherical object [13].....	11
3.1	The schematic illustrations of the proposed Bi Pyramid dimer .....	16
3.2	The refractive index (a) and the density protein layers after 30 min of adsorption are plotted as a function of the molecular weight.....	17
3.3	Ribbon model structure of lysozyme (Lys) protein .....	19
3.4	Ribbon model structure of human serum albumin (HSA) protein.....	20
3.5	Ribbon model structure of human immunoglobulin.....	21
3.6	Ribbon model structure of human fibrinogen (Fb) protein .....	22
4.1	TE and TM mode excitation peaks.....	30
5.1	LSPR peaks for different aspect ratio .....	35
5.2	LSPR extinction peaks for gold and silver.....	37
5.3	Electric field enhancement for gold (left) and silver (right).....	37
5.4	LSPR extinction spectra for a) Copper b) Sodium c) Aluminum d) Potassium....	38
5.5	Electric field enhancement of Sodium .....	39
5.6	LSPR extinction peaks for a) Zirconium Nitride b) Titanium Nitride c) Hafnium Nitride d) Tantalum Nitride.....	41
5.7	Electric field enhancement for Titanium Nitride.....	41
5.8	LSPR extinction peaks for AZO, GZO and ITO.....	43
5.9	Electric field enhancement for AZO.....	43
5.10	LSPR peaks for different materials and FOM calculation .....	45



# List of Tables

4.1 Characteristics of proteins .....	26
5.1 Effects of peak shifts due to change in aspect ratio.....	34
5.2 LSPR peaks for different materials and FOM calculation.....	45

# Acronyms

<b>LSPR</b>	Localized Surface Plasmon Resonance
<b>BP</b>	Bi- Pyramid
<b>DDA</b>	Discrete Dipole Approximation
<b>FEM</b>	Finite Element Method
<b>FDTD</b>	Finite Difference Time Domain
<b>Au</b>	Gold
<b>Ag</b>	Silver
<b>Cu</b>	Copper
<b>Na</b>	Sodium
<b>K</b>	Potassium
<b>Al</b>	Aluminium
<b>ZrN</b>	Zirconium Nitride
<b>HfN</b>	Hafnium Nitride
<b>TaN</b>	Tantalum Nitride
<b>TiN</b>	Titanium Nitride
<b>ITO</b>	Indium Tin Oxide
<b>AZO</b>	Aluminum zinc oxide
<b>GZO</b>	Galium Zinc Oxide
<b>PML</b>	Perfectly Matched Layer
<b>TE</b>	Transverse Electric
<b>TM</b>	Transverse Magnetic
<b>DFT</b>	Discrete Fourier Transform
<b>RIU</b>	Refractive Index Unit

# Chapter 1

## 1.1) INTRODUCTION:

### **LOCALIZED SURFACE PLASMON RESONANCE (LSPR):**

There are many different types of materials that exhibit a large negative real and small positive imaginary dielectric function. This kind of materials has the ability of supporting a collective excitation of the conduction electrons known as plasmon excitation. In metal nanoparticles this leads to a localized surface plasmon resonance known as LSPR. This phenomenon is the outcome of the generation of strong peaks in excitation spectra and strong enhancements of the local electromagnetic fields surrounding the nanoparticles [1]. In practical, LSPR based instruments use a broad band white light source like LED to lighten the nanoparticle sensor substrate. A spectrometer performs as the detector and can be placed for transmission or reflection purposes. The spectrometer gives a extinction spectrum of the sensor substrate.[2]

## 1.2 IMPACT & APPLICATIONS:

Nano devices showing various electronic, photonic, chemical and biomedical properties need to be evolved for the purpose of coming age of electronic sensors. The use of noble metal nanostructures in these Nano devices is promising in field of highly sensitive optical Nano sensors,

photonic components and in surface-enhanced spectroscopies because of the large extinction cross section and photosensitivity they display [3].

Nanotechnology, including Nano scale detection, photo thermal tumor therapy, Nano rotors and thermoelectric solar cells etc are affected vastly by the efficient control of local photo thermal energy deposition at the nanoscale.[4]

It has always been a challenge to develop low cost, portable devices that can provide fast, reproducible, sensitive and selective sensing for applications for the control of diseases, agricultural quality and the quality of the environment. Many current sensors in this fields are expensive, large in volume and complex production procedures. On the other hand, LSPR sensors offer high sensitivity, a small footprint and reasonably affordable due to its simplicity of fabrication [5].

Medical-oriented bio-sensors are expected to evolve mainly in following directions [5]:

- i. Higher sensitivity
- ii. Cellular, intercellular and tissue level detection
- iii. Combination of current nanostructures with other materials
- iv. Early detection of heart diseases and cancer
- v. Detection of the HIV-1 virus
- vi. Ultra-sensitive influenza detection through antigen-antibody interaction using LSPR
- vii. The diagnosis of pregnancy related conditions like preeclampsia

Impact in agricultural and environment [5]:

- i. Improving the use of soil, water and fertilizer

- ii. Improving crop resistance to disease
- iii. Ability to monitor environment for contaminants and pollutants for the improvement of agricultural techniques
- iv. Ability to monitor plant nutrients allows the yield and quality of crops to be improved

### **1.3 MOTIVATION:**

LSPR implementations in various applications like highly sensitive Nano sensors, photonic components and surface-enhanced spectroscopies are largely based on the position of the LSPR excitation maximum  $\lambda_{max}$ . This peak in excitation is reactive to the size, shape, inter-particle spacing, dielectric environment and dielectric properties of the nanoparticles. As the noble nanoparticles such as Gold (Au) and Silver (Ag) provide strong extinction and scattering spectra throughout the UV, visible and near IR spectrum, most researchers and scientists use Au and Ag in theoretical, experimental and the development of LSPR applications. There are a number of other materials may show strong peaks in excitation spectra and also strong enhancements of the local electromagnetic fields nearby the nanoparticles. But very little work has been done using other materials. So we are motivated to do simulation based research to provide a comprehensive and relative comparison for material performance and to evaluate the performance of Nano bi-pyramid structure using various materials.

## 1.4 PROBLEMS:

The requirement for LSPR is a large negative real and a small imaginary dielectric function as the real part of dielectric function defines the strength of the polarization induced by an external electric field and imaginary part describes the losses encountered in polarizing the material [6]. So theoretically a large number of other materials should support plasmon resonance. However, most of these metals are either unstable, difficult to work with or prone to surface oxidation that can significantly affect the optical properties [3]. Because of these problems generally noble metal nanoparticles like Gold (Au) and Silver (Ag) are used for development, research and in applications of LSPR instead of other materials. Gold has larger mean relaxation time of conduction electron than Silver and used for lower near-infrared frequencies. Gold is vastly used for being chemically stable in different environment. However, Gold has high inter band losses in the visible spectrum for wavelength below or about 500 nm. Similarly Copper (Cu) has large inter band losses over most of the visible spectrum [6]. As future plasmonic applications require even lower losses to fully explore their potential, alternative materials with lower losses need to be used.

## **1.5 THESIS OVERVIEW:**

In our Thesis, FDTD simulation based analysis is done by using nano bi-pyramid structure of different materials made of Aluminum (Al), copper (Cu), noble metals like Gold (Au) and silver (Ag), alkali metal like Sodium (Na) and Potassium (K), Transition Metal Nitrides such as Zirconium Nitride (ZrN), Titanium Nitride (TiN), Hafnium Nitride (HfN), Transparent Conductive Oxides (TCOs) such as AZO, GZO, ITO. We also use different protein like Lysosome, Fibrinogen, Immunoglobulin and Human Serum Albumin. We have computed extinction and electric field intensity using Mie calculation and created database containing sensitivity and Figure of Merit so that this data can later be used for fabrication process and application based on these materials.

## Chapter 2

# Theoretical Background of LSPR

### 2.1 LSPR THEORY:

Nanoparticles of dimensions below 100 nm show fascinating properties in nano-systems which are not observed in ordinary materials. Additionally, metallic conductive NPs with size smaller than the wavelength of surrounding light show strong dipolar excitations in the form of localized surface plasmon resonances (LSPR). LSPRs are non-propagating excitations of the conduction electrons of metallic nanostructures coupled to the electromagnetic field. The curved surface of the particle deploys an effective restoring force on the driven electrons which eventually creates resonance leading to field amplification both inside and in the near-field zone outside the particle. This resonance is called the *localized surface plasmon* or short *localized Plasmon* resonance. Another effect of the curved surface is that plasmon resonances can be excited by direct light illumination, in contrast to propagating Surface Plasmon Polaritons (SPPs) [7].

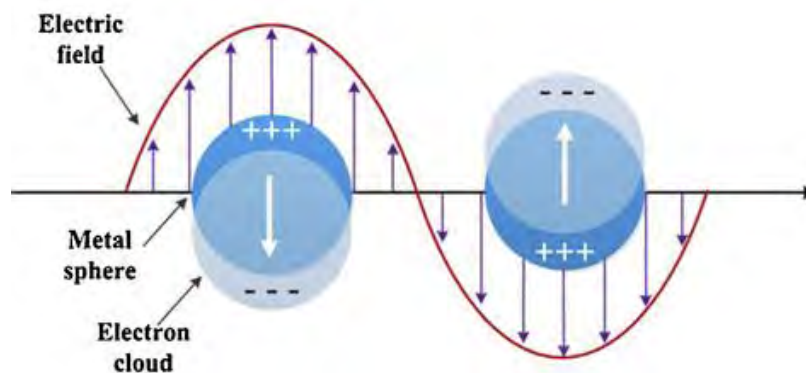


Fig 1.1: illustration of the excitation of localized surface plasmon resonance [8]



As LSPR is the coupling of non-propagating excitations of the conduction electrons and the electromagnetic field surrounding the nanoparticle, this causes LSPR to have three unique optical properties [9],

- i. The field intensity outside the nanoparticle is the greatest at the surface and fading with distance
- ii. The optical extinction is maximum at the resonance wavelength, determined by the particles shape, composition and the refractive index of the surrounding medium.
- iii. The extinction peak shifts when the refractive index of the surrounding medium is changed.

For gold and silver nanoparticles, the resonance falls into the visible region of the electromagnetic spectrum. Because of this, bright colors exhibited by particles both in transmitted and reflected light, due to resonantly enhanced absorption and scattering. This effect has found applications for many hundreds of years, for example in the staining of glass for windows or ornamental cups [7].



**Fig 1.2: Lycurgus cup, a piece of Ancient Roman Nanotechnology [10]**

## 2.1 Drude Model:

In the early 1900 Paul Drude applied the kinetic theory of gasses to a metal. This Model is a purely classical model of electronic transport in conductors. It describes the collisions between freely moving electrons and a lattice of heavy, stationary ionic cores. It provides a very good approximation of the conductivity of noble metals. The electrical polarization can be described by the materials complex electrical permittivity or dielectric function denoted by  $\varepsilon(\omega)$  [6]. To find the functional form of the LSPR peak wavelength's dependence on the dielectric function of the medium, one can use the analytical, frequency-dependent form for  $\varepsilon(\omega)$  from the Drude Model of the electronic structure of metals:

$$\varepsilon(\omega) = 1 - \frac{\omega_p^2}{\omega^2 + \gamma^2}$$

Here  $\omega_p$  is the plasma frequency and  $\gamma$  is the damping parameter of the bulk metal. For visible and near-infrared frequencies where the frequency is close to plasma frequency damping can be neglected as  $\gamma \ll \omega_p$ . So the above equation can be simplified to:

$$\varepsilon(\omega) = 1 - \frac{\omega_p^2}{\omega^2}$$

According to the generalized Drude Theory the dielectric function can be written as:

$$\varepsilon(\omega) = \varepsilon_1(\omega) + i\varepsilon_2(\omega)$$

Here  $\varepsilon_1(\omega)$  is the real part and  $\varepsilon_2$  is the imaginary part of the dielectric function. This real part describes the strength of the polarization induced by an external electric field and imaginary part shows the losses encountered in polarizing the

material. At optical frequencies  $\varepsilon(\omega)$  can be experimentally determined via reflectivity studies.

Using the expression of  $\varepsilon(\omega)$  for the resonance condition where  $\varepsilon(\omega) = -2\varepsilon_m$  the following can be obtained:

$$\omega_{max} = \frac{\omega_p}{\sqrt{2\varepsilon_m + 1}}$$

Here  $\omega_{max}$  is the LSPR peak frequency. Converting from frequency to wavelength via  $\lambda = 2\pi c/\omega$ , and then from dielectric constant to index of refraction via  $\varepsilon_m = n^2$ , the above expression becomes :

$$\lambda_{max} = \lambda_p \sqrt{2n_m^2 + 1}$$

Here  $\lambda_{max}$  is the LSPR peak wavelength and  $\lambda_p$  is the wavelength corresponding to the plasma frequency of the bulk metal. Thus, we see that the dependence of LSPR peak wavelength on the refractive index ought to be approximately linear at optical frequencies which are used in the experiments [11].

## 2.3 Mie Theory:

In 1908 Gustav Mie solved Maxwell's equations for the case of scattering and absorption of light by particles of spherical shapes. The correct boundary conditions for electromagnetic fields at the metallic NP and its surrounding is applied to a plane wave incident on a homogeneous conducting sphere gives the following total scattering, extinction and absorption cross section:

$$\sigma_{sca} = \frac{2\pi}{|k|^2} \sum_{L=1}^{\infty} (2L+1)(|a_L|^2 + |b_L|^2)$$

$$\sigma_{ext} = \frac{2\pi}{|k|^2} \sum_{L=0}^{\infty} (2L+1)Re\{a_L + b_L\}$$

$$\sigma_{abs} = \sigma_{ext} - \sigma_{sca}$$

Here the parameters  $a_L$  and  $b_L$  are defined as:

$$a_L = \frac{m\psi_L(mx)\psi'_L(x) - \psi'_L(mx)\psi_L(x)}{m\psi_L(mx)\chi'_L(x) - \psi'_L(mx)\chi_L(x)}$$

$$b_L = \frac{\psi_L(mx)\psi'_L(x) - m\psi'_L(mx)\psi_L(x)}{\psi_L(mx)\chi'_L(x) - m\psi'_L(mx)\chi_L(x)}$$

Where  $k$  is the incoming wave vector and  $L$  are integers representing the dipole to higher multipoles of the scattering. Here,  $m = \tilde{n}/n_m$ , where  $\tilde{n} = n_R + in_I$  is the complex refractive index of the metal and  $n_m$  represents the real refractive index of surrounding medium. Also  $x = k_m r$  where  $r$  is the radius of the particle.  $k_m = 2\pi/\lambda_m$  is defined as the wavenumber in the medium rather than the vacuum wavenumber. The Ricatti-Bessel function  $\Psi_L$  and  $\chi_L$  are defined in terms of the half-integer-order Bessel function of first kind  $\left(J_{n+\frac{1}{2}}(z)\right)$ ,  $\Psi_n(x) = \left(\frac{rx}{2}\right)^{0.5} \left(J_{n+\frac{1}{2}}(x)\right)$  and  $\xi_n(x) = \left(\frac{rx}{2}\right)^{0.5} H_{n+\frac{1}{2}}(x)$ ,  $H_{n+\frac{1}{2}}(x)$  is the half-integer-order Hankel function of the second kind [11,12].

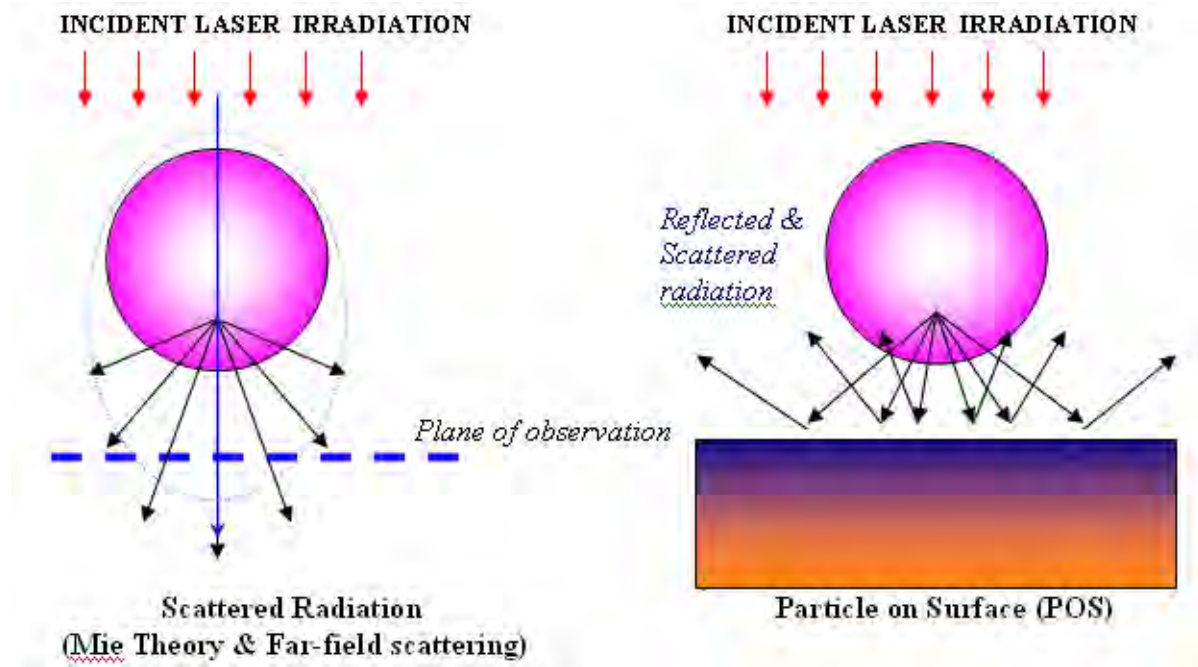


Fig 1.3: Schematics illustration of scattering and absorption spherical object [13]

## 2.2 GANS THEORY:

Mie theory as formulated above is strictly applicable to spherical particles. In 1912, Richard Gans generalized Mie's result to spheroidal particles of any aspect ratio in the small particle approximation. He found that the absorption cross section for a prolate spheroid is,

$$\sigma_{abs} = \frac{\omega}{3c} \varepsilon_m^{3/2} V \sum_j \frac{(1/P_j^2) \varepsilon_2}{\{\varepsilon_2 + [\frac{1-P_j}{P_j}] \varepsilon_m\}^2 + \varepsilon_2^2}$$

Here the sum over  $j$  considers the three dimensions of the particle.  $P_j$  includes  $P_A$ ,  $P_B$ ,  $P_C$ , termed depolarization factors, for each axis of the particle, where  $A > B = C$  for a prolate spheroid, the depolarization factors anisotropically alter the values of  $\varepsilon_1$  and  $\varepsilon_2$  and the resulting LSPR peak frequencies. Explicitly, they are:

$$P_A = \frac{1 - e^2}{e^2} \left[ \frac{1}{2e} \ln \left( \frac{1 + e}{1 - e} \right) - 1 \right]$$

$$P_B = P_C = \frac{1 - P_A}{2}$$

Where  $e$  is the following factor, which includes the particle aspect ratio  $R$ :

$$e = \left[ 1 - \left( \frac{B}{A} \right)^2 \right]^{1/2} = \left( 1 - \frac{1}{R^2} \right)^{1/2}$$

The extinction spectrum resulting from  $\sigma_{abs}$  has two peaks, one corresponding to the transverse plasmon mode from the  $x$  and  $y$  contributions to the sum, and the other corresponding to the longitudinal plasmon mode from the  $z$  contribution. Equation of  $\sigma_{abs}$  also provides an intuitive understanding of the effect of aspect ratio on the LSPR peak wavelength. The factor weighting  $\varepsilon_m$ , which is 2 for spherical

particles, is  $\left[\frac{1-P_j}{P_j}\right]$ , a quantity that increases with aspect ratio and can be much greater than 2. This leads to a red-shift of the plasmon peak with increasing aspect ratio, as well as increased sensitivity to the dielectric constant of the surrounding medium.

If we consider working with complex particles then, it cannot be calculated analytically so we must be study it numerically. There are various types of Numerical methods for plasmonic nanoparticles include finite difference time domain (FDTD), discrete dipole approximation (DDA), and finite element method (FEM) [11].

## **2.5 Summary:**

This chapter discusses the basics of LSPR. Drude Model provides a detail study of the dielectric properties of metal nanoparticles. Mie theory provides an analytical model for scattering and absorption of light by spherical particles. Gans theory is a modified form of Mie theory which is used for modeling spheroidal shape particles. Beyond sphere and spheroid, particle shape plays an important role in determining the LSPR peak.



## Chapter 3

### Structure Design and Analysis:

#### 3.1 Introduction:

Research interests for noble metal nanoparticles have risen exponentially in the last decades especially for Au [14-19] and Ag [20-23], due to their interesting optical properties. Generally, LSPR is derived from the inherent interaction between free electrons of these metal NPs and incident electromagnetic wave [24], which in turn leads to large optical absorption [25], strong Rayleigh scattering [26], and enhanced electronic field coupling [26, 27]. As a result, applications of Ag and Au nanostructures have surged, including chemical and biochemical sensing [28-31], medical diagnostics [32], therapeutics [33], waveguides [34], optical devices [35] and surface-enhanced spectroscopies [36-38]. However, alternative materials like different metals, transition metal nitrides and TCO have also been considered for use.

Recently, a number of studies have been extensively done on Nano sphere core coated by various metals, transition metal nitrides and transparent conducting oxides to explore its plasmonic applications. However, Nano bipyramids provide greater sensitivity than conventional Nano spheres due to the increasing local field enhancement near the tip of the bi pyramid. As a result, a significant field enhancement is possible for much sensitive detection if a biomolecule is placed in the tip of the bi pyramid. Above all, a detailed analysis of the sensitivity performance for different biomolecule detection is still unavailable

## 3.2 Proposed Structure:

The Bi pyramid structure was designed and run on Lumerical FDTD solutions. The structure is first drawn in the CAD window. The physical properties of the structure is defined such as length, Width, tip radius, cone angle of the pyramid. The model contains two pyramids attached together by the base. The angle orientation of one pyramid is opposite of the other. The two tips of the bi-pyramid are designed as spheroidal shapes to sharpen the electric field enhancement. The tip radius of the BP is 3.5nm. The length of Bi pyramid is considered 105 nm and the width of the Bi pyramid is 35 nm. The cone angle of the bi pyramid is 29.5 degree.

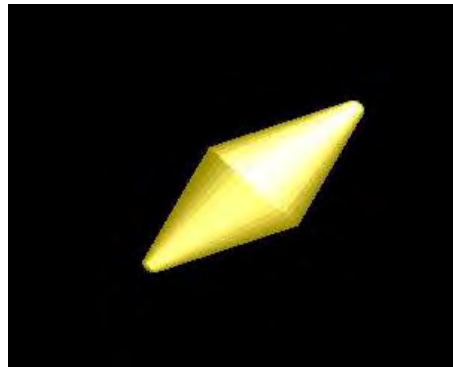


**Fig. 3.1 The schematic illustrations of the proposed Bi-Pyramid dimer.**

The whole structure has been placed on a SiO<sub>2</sub> substrate within a buffer solution. In our work, we have used a number of proteins as biomolecules ranging from a

molecular weight of 14.3 kDa to 390 kDa to be adsorbed in the tip of the bi pyramids. The biomolecules were modeled by using the refractive indices found in the figure below.

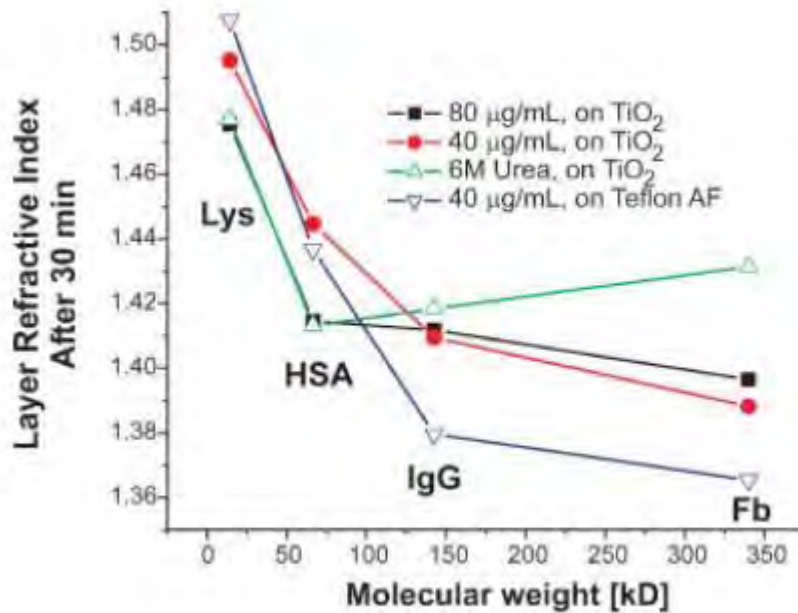


**Figure 3.2 The refractive index (a) and the density protein layers after 30 min of adsorption are plotted as a function of the molecular weight [ 40]**

Usually, A laser light source is used to excite the surface Plasmon to calculate the absorption cross-section or scattering cross section. With a broadband spectrum,

significant red shifts would be found at the resonant peaks in presence of protein samples.

### **3.3 Protein as a Biomolecule:**

A bio-marker is usually referred to a measurable indicator of some biological state or condition. The term is also occasionally used to refer to a substance, the presence of which indicates the existence of a living organism [41]. Proteins detected as biomarkers can benefit a number of scientific and clinical applications such as drug research and environmental monitoring, early disease diagnosis and treatment such as prostate specific antigen (PSA) protein for prostate cancer detection [42]. There are different types of biomarkers ranging from small molecules (i.e., PSA and lysozyme) to large molecules (i.e., Fibrinogen and tenascin).

In this thesis, we have investigated the effect of using different protein which can be used as potential biomarkers. The samples are:

### 3.3.1 Lysozyme (Lys):

Lysozyme[43], also known as muramidase or N-acetylmuramide glycanhydrolase is an antimicrobial enzyme produced by animals that forms part of the innate immune system. Lysozyme is a glycoside hydrolase that catalyzes the hydrolysis of 1,4-beta-linkages between N-acetylmuramic acid and N-acetyl-D-glucosamine residues in peptidoglycan, which is the major component of gram-positive bacterial cell wall.<sup>[5]</sup> This hydrolysis in turn compromises the integrity of bacterial cell walls causing lysis of the bacteria. Lysozyme is abundant in secretions including tears, saliva, human milk, and mucus. It is also present in cytoplasmic granules of the macrophages and the polymorphonuclear neutrophils (PMNs). Large amounts of lysozyme can be found in egg white. Serum lysozyme can be used as a potential biomarker of monocyte/macrophage activity in rheumatoid arthritis.

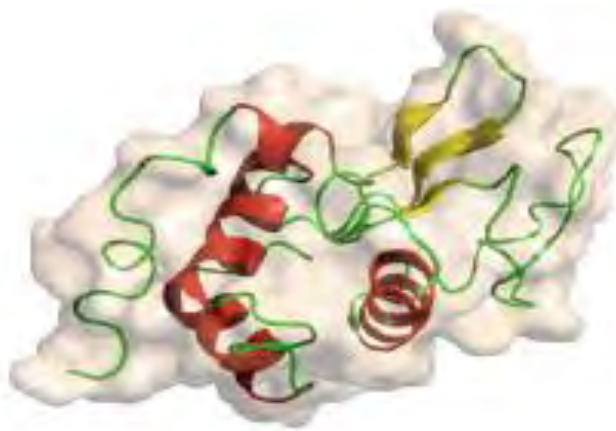


**Figure 3.2: Ribbon model structure of lysozyme (Lys) protein [44]**

### 3.3.2 Human serum albumin (HSA):

Human serum albumin (HSA) is the version of serum albumin found in human blood. It is the most abundant protein in human blood plasma. It transports hormone, fatty acids and other compounds, buffer pH and maintains oncotic pressure, among other functions. HSA is currently used for investigating human exposure to xenobiotic compounds, including therapeutics and environmental pollutants. A recent study executes that mycotoxin, i.e., satratoxin G (SG) adducts on HSA may serve as biomarkers of exposure to *Stachybotrys chartarum*[45].



**Figure 3.3: Ribbon model structure of human serum albumin (HSA) protein[46]**

### 3.3.3 Human Immunoglobulin (IgG):

Immunoglobulin (IgG)[47] is a substance made from human blood plasma. The plasma, processed from donated human blood contains antibodies that protect the body from diseases, such as hepatitis, chickenpox, or measles. They are the smallest but most common antibody (75% to 80%) of all the antibodies in the body. IgG has been found to be a potential biomarker for acute coronary syndrome (ACS) in adults.



**Figure 3.4: Ribbon model structure of human  $\gamma$ -immunoglobulin (IgG) protein[48]**

### 3.3.4 Human Fibrinogen (Fb):

Fibrinogen (Fb)[49] is a soluble, large glycoprotein in vertebrates that helps in the formation of blood clots. It is one of the 13 coagulation factors responsible for normal blood clotting. Low level of Fb can cause thrombosis leading to serious medical condition, such as heart attack and stroke. Current research reveals its potential functionality as a biomarker for inflammation due to coronary artery disease [50].

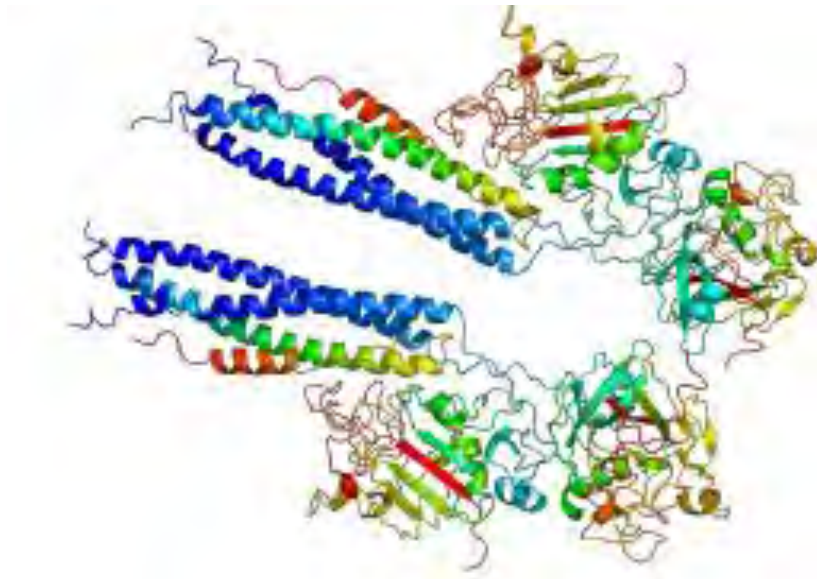


**Figure 3.6: Ribbon model structure of human Fibrinogen (Fb) protein[50]**



### **3.4 Summary:**

In this chapter we have proposed a Nano bipyramid for better sensitivity performance. A bipyramid structure modeled as metals, transition metal nitrides and transparent conduction oxides to enhance the electric field coupling at the tip region. It is expected to produce higher plasmonic shifts in the absorption spectra when a biomolecule is adsorbed in the tip of the structure. A small number of proteins which are potential biomarker for various diseases have been selected as bio sample.

## Chapter 4

### FDTD Simulation

#### 4.1 Introduction:

Finite difference time domain (FDTD) is a numerical method for solving Maxwell's equations in arbitrary metallic/dielectric structures. The basic principle is to discretize the simulation space into nodes and substitute the curl equations and partial time differentials of Maxwell's equations with finite central differences in both spatial domain and time domain [51]. In the FDTD technique, Maxwell's curl equations are discretized by using finite difference approximations in both time and space that are easy to program and are accurate. To achieve high accuracy for realizing the spatial derivatives involved, the algorithm positions the components of the electric and magnetic field about a unit cell of the lattice that constitutes the FDTD computational domain. Each individual cube in the grid is called the Yee cell [52]

Lumerical FDTD solutions software was used in order to create a Nano particle in the shape of a bipyramid. Generally, softwares like FDTD are used to simulate complex structures. In this chapter we observe the LSPR mechanism by analyzing our model in Fig. 3.1 using FDTD method.

## **4.2 Material Modeling:**

The most important part of our simulation was to model the materials we used. The whole geometry of the structure was used as a single material. The material was modeled by using experimental values real and complex refractive index of different materials measured at sampled wavelength values. In our thesis, The permittivity data for different material used in this simulation was sourced from the optical Au[53],Ag[53],Na[54],K[54],Al[54],Cu[54],Zrn[55],TiN[55],Hfn[55],AZO[55],ITO[55],GZO[55].For our simulation, the refractive index of background buffer has been chosen as 1.332 .

## **4.3 Biomolecule Modeling:**

The modeling of the biomolecules is another important topic for consideration. . In this study, we have taken protein samples with significant difference molecular weight ranging from 14.3 kDa to 390 kDa. The adsorption of chicken egg white lysozyme (Lys), human serum albumin (HSA), human -immunoglobulin (IgG), and human Fibrinogen (Fb) have been modeled on glass substrate in the tip of bi pyramid. The refractive index used for modeling the biomolecule was used from the experimental analysis [56, 57]. The sizes, shapes and RI values of these modeled bio samples are shown in the following table:

<b><u>Protein</u></b>	<b><u>Dimension</u></b> <b>(nm)</b>	<b>Mass</b> <b>(kDa)</b>	<b>Refractive</b> <b>Index</b>
Lys	2 x 2 x 2	14.3	1.5
HSA	8 x 7 x 4	66	1.45
IgG	4 x 3.6 x 3	148	1.42
Fb	46 x 3 x 6	390	1.39

**Table 4.1: Characteristic of the simulated proteins**

#### **4.4 Mesh Varying Test:**

The validation for the FDTD simulation is done by comparing results of the simulation with the experimental and theoretically predicted values. To maintain the accuracy and stability of the FDTD calculations, mesh independence test has been performed by finding the correct mesh size. The threshold mesh size is the largest grid size to accurately model the system without being computationally prohibitive. Generally, it is obtained by convergence testing. We started with a very small mesh size, then it was increased until the simulation results diverged. The threshold mesh size is the lowest size which gives the diverging results [58]. We chose a spatial mesh size of 1 nm, as because it is smaller than the threshold mesh size (0.75 nm) and the halving of this mesh size, although increases the simulation time considerably, yields same results. For different materials used in the simulation the mesh size was varied from 1nm to 2nm. The algorithm of FDTD requires the time

increment have a specific bound relative to the spatial discretization (grid/mesh size) to ensure the stability of the time-stepping algorithm. In our simulation we used 300 fs for total simulation time with a minimum time step of 0.00095 fs.

## **4.5. Boundary Conditions:**

Boundary conditions denote how the field quantities should behave as they reach the edge of the simulation region. For our simulation purpose, mainly two sets of boundary condition were used. One is perfectly matched layer (PML) and the other is Symmetric/Asymmetric.

### **4.5.1 Perfectly Matched Layers:**

Perfectly matched layer (PML) denotes the boundary condition that ensures that outgoing radiations that reach the edge of the simulation boundary will die out at the boundary without reaching back into the simulation region to interfere with the field inside. An ideal PML boundary will absorb all of the electromagnetic field incident on it. However, this does not happen in real PML condition. Depending on the number of layers, a real PML can only approximate an ideal PML boundary with different accuracy. While the absorption is maximum in case of normal incidence, oblique incidence can result in significant reaction back into simulation region. So

number of layers must be chosen carefully in a t he direction of interest to simulate the practical scenario as accurately as possible. In our simulation we have taken 4 layers to provide consistency with the experimental results. Also this boundary condition works best if the structure is extended through the simulation boundary. PML boundary is used to simulate and study the behavior of an isolated structure. If a structure is surrounded by a simulation region with PML boundary condition imposed on every side, it can be assumed to be isolated. The only excitation source will be the source placed within the boundary. The electromagnetic field profile observed after simulation will be only due to the size of the structure alone [58].

#### **4.5.2 Symmetric/anti-symmetric:**

Symmetric/anti-symmetric boundary conditions are used when the user is interested in a problem that exhibits one or more planes of symmetry; both the structure and source must be symmetric. Symmetric boundaries are mirrors for the electric field, and anti-mirrors for the magnetic field. On the other hand, antisymmetric boundaries are anti-mirrors for the electric field, and mirrors for the magnetic field. Careful consideration must be given to whether symmetric or anti-symmetric boundary conditions are required, given the vector symmetry of the desired solution. For meaningful results, the sources used must have the same symmetry as the boundary conditions [58 ].

## 4.6 Optical Sources:

The main part of our simulation consists of the light source. In our simulation we have used the Total Field Scattered Field source (TFSF source) which is particularly used for understanding the behavior of scattering and absorption from small particle. It is also convenient to properly evaluate the electric field enhancement at the edges of bi pyramid structure. A TFSF source is modeled in such a way that it splits the simulation region in two different regions.

### (a) Total Field Region:

It contains the total field of (the summation of absorbed and scattered light; which is also known as the extinction as discussed in chapter 1).

(b) **Scattered Field Region:** It only contains the scattered light.

Within the boundary of the source it is a plane wave that propagates with a wave vector normal to its surface of incidence. At the edge of the boundary the absorbed field is subtracted from the total field leaving only the scattering field to propagate outside. When it acts as a plane wave it can be defined to have a fixed polarization. Depending on the angle of polarization it will give TE (for angle 90) or TM (for angle 0) wave propagation in 3D simulation [58]. The extinction spectra for a gold particle was normalized with respect to the maximum extinction value for the TE mode and TM mode which is shown in Figure 4. . In the TE mode ( we know that the main field components are  $E_y, H_x, H_z$ ) there is extinction peak at 800nm as this

mode excites resonances in y direction and thus excites only one LSPR mode in the gold nanoparticle, as indicated in Figure 3.4(b). However, for the TM mode (The main field components are  $E_x, E_z, H_y$ ), two extinction peaks are visible because TM polarization excites resonances in both the X and Z directions, as indicated in Figure 3.4(b). There is an extinction peak around 690 nm for both TE and TM mode because the circular shape of a gold nano particle supports degenerate modes [59].

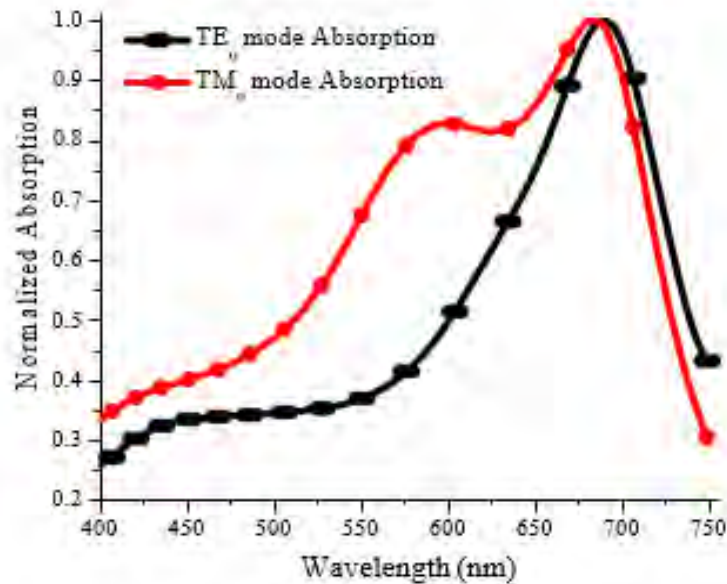


Fig 4.1 TE and TM mode excitation peaks [59 ]



Our main goal was to tune the LSPR peak for sensor applications. Therefore, we used TE mode in our simulation as it excites one LSPR peak. TM mode is a mixture of two different LSPR peaks which can increase the complexity in understanding the peak shifting of the bipyramid. Therefore, all our simulation was used with TE mode excitation.

## 4.7 Power Absorption and Scattering:

In our simulation we used two different analysis groups for calculating absorption and scattering power. The scattering analysis group contains the scattered light from the bipyramid. The scattering cross section calculation is denoted by as follows:

Scattering analysis group:

- Total power scattering outwards,
- Unit= W
- $P_{scat} = (P_{x1} + P_{x2} + P_{y1} + P_{y2} + P_{z1} + P_{z2}) * sourcepower(f)$
- $Cross\_section = P_{scat} / source\ intensity(f)$

The absorption analysis group calculates the absorbed light from the source. The absorption

Cross section calculation is as follows:

Absorption analysis group:

- Total power absorbed.
- Unit= W
- $P_{abs} = (P_{x1} + P_{x2} + P_{y1} + P_{y2} + P_{z1} + P_{z2}) * sourcepower(f)$
- $Cross\_section = P_{abs} / source\ intensity(f)$

## **4.8 Summary:**

FDTD solution is a numerical method that can simulate general to complex structures. Increasingly, engineers and scientists in non-traditional electromagnetics-related areas such as photonics and nanotechnology have become aware of the power of FDTD techniques. Here we have simulated the bipyramid structure for exploring its bio-sensitivity by complete 3D FDTD method for. FDTD has leded us to results that are theoretically and experimentally expected. Simulation of much complicated photonics structures for biomolecule detection will be possible with FDTD method.

## **Chapter 5**

### **Simulation and Result Analysis**

#### **5.1 Introduction:**

In theoretical investigations, power absorption and scattering are usually studied to find out the characteristics of LSPR biosensors. In addition, we will also see that for different biomolecules the resonance peak will shift. We have also calculated to find out the sensitivity of bipyramid. In our analysis, we have considered extinction cross-section rather than scattering or absorption. Extinction cross section is the summation of absorption and scattering cross section. The aspect ratio and background refractive index change have been varied to observe the effects on the extinction spectrum and electric field coupling in the tip region. The optical source has been placed at 90 degrees(TM mode excitation). We have used some protein as samples. The surrounding environment of the simulation and structure executes a proper experimental setup. The LSPR shifts calculated from the results will give us a better understanding of sensitivity of the bipyramid structure.

## 5.2 Aspect Ratio:

The Aspect ratio usually means the width of the particle divided by the length of the particle. The aspect ratio change results the LSPR peak to shift. For a length of 35nm and a width of 70nm we can see a peak at 724.4 nm as a gold bipyramid. when width is 87.5 the peak is at 764 nm. If we keep increasing the ratio we can see that the peak shifts. The table and below represents the effects of change in LSPR peak due to change aspect ratio.

GOLD bipyramid Width	Aspect ratio = W/L	Extinction cross sections(nm)
70	2	724.39
87.5	2.5	764
115	3	800
140	4	865.049

**Table 5.1 Effects of Peak shifts due to change in aspect ratio**

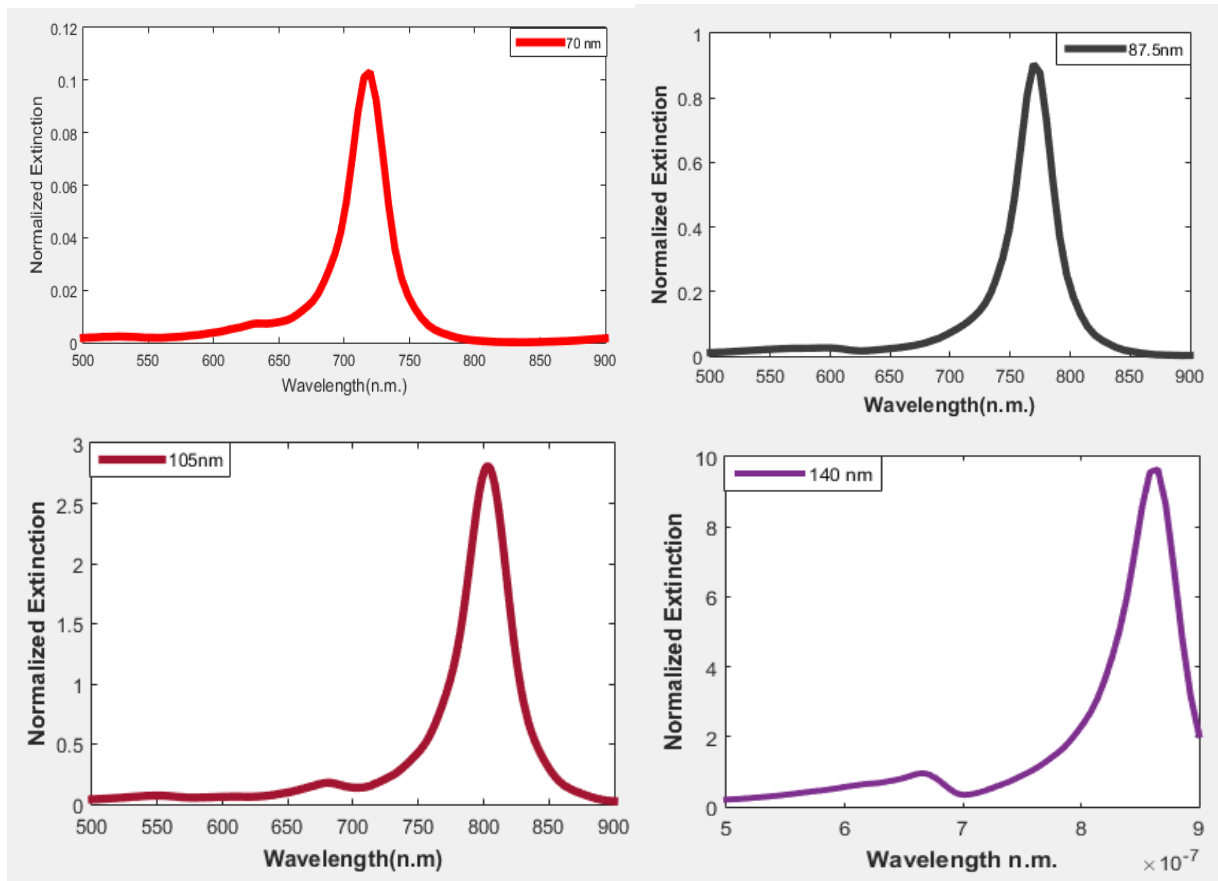


**Figure 5.1 The LSPR peaks for 1) width 70nm. 2) Width 87.5nm 3) width 105nm 4)140nm due to change in aspect ratio**

### **5.3 Noble metals:**

Noble metals such as gold and silver have been used extensively over the years for plasmonic applications. In our simulation we have modeled our bipyramid as gold and silver. For Gold bipyramid we can see that the LSPR peak is found at 800nm. However, for silver we see a LSPR peak at 906nm. As a result, we can see that silver has a much sharper peak than gold and if we calculate the electric field profile we can see that electric profile field for silver much higher than gold. Consequently, this shows that silver much more efficient than gold. Gold and silver both have been in use for plasmonic and metamaterial devices for a year.

However, at optical frequencies interband transitions occur important role in these metals [60]. Silver and gold both have their pros and cons. Silver and gold both have losses in the visible and near infrared spectra. However, silver is chemically unstable. Both of them are costly. The extinction peaks and electric field enhancement of both gold and silver are shown below.

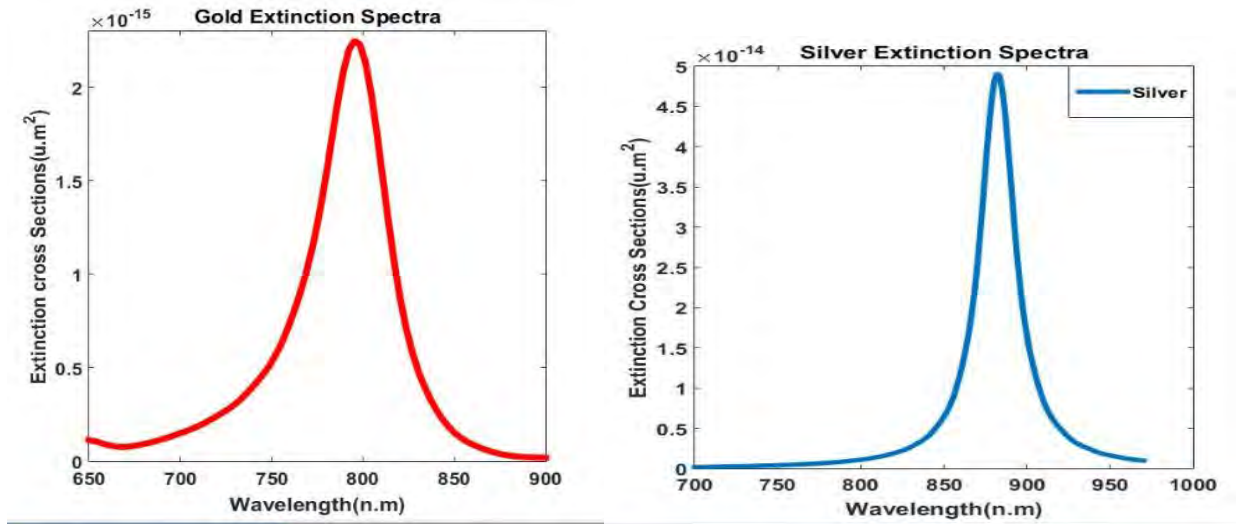


**Figure 5.3 LSPR extinction peaks for gold and silver**

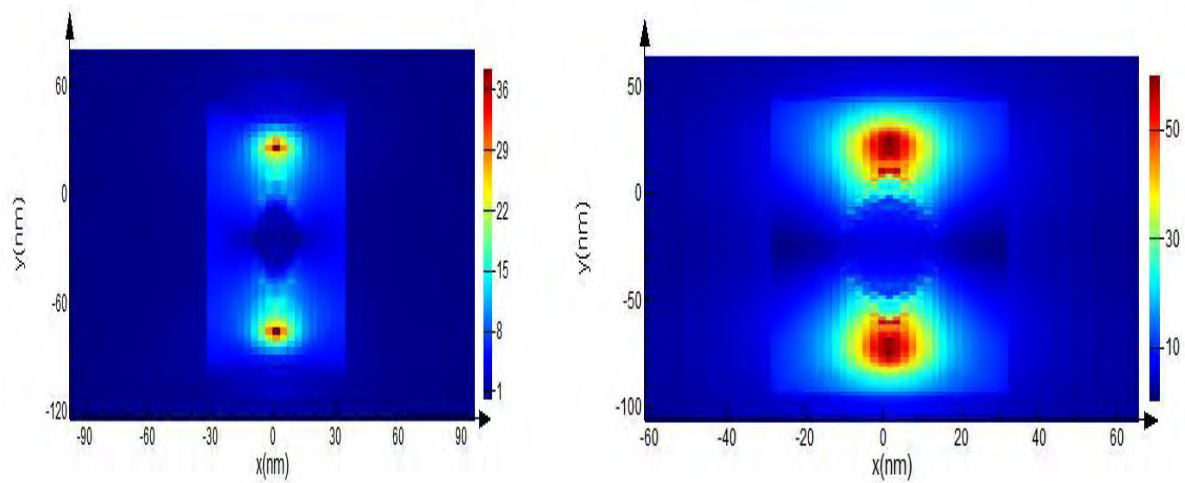


**Figure 5.4 Electric field enhancement for gold (left) and silver (right)**

## 5.4 Conventional Metals:

In our simulation, we have also used copper, sodium, aluminum, potassium as material for bipyramid. Copper has a LSPR peak of 788nm, Sodium has a LSPR peak of 662 nm, Aluminum has a LSPR peak of 630 nm and Potassium has a LSPR peak of 761 nm.

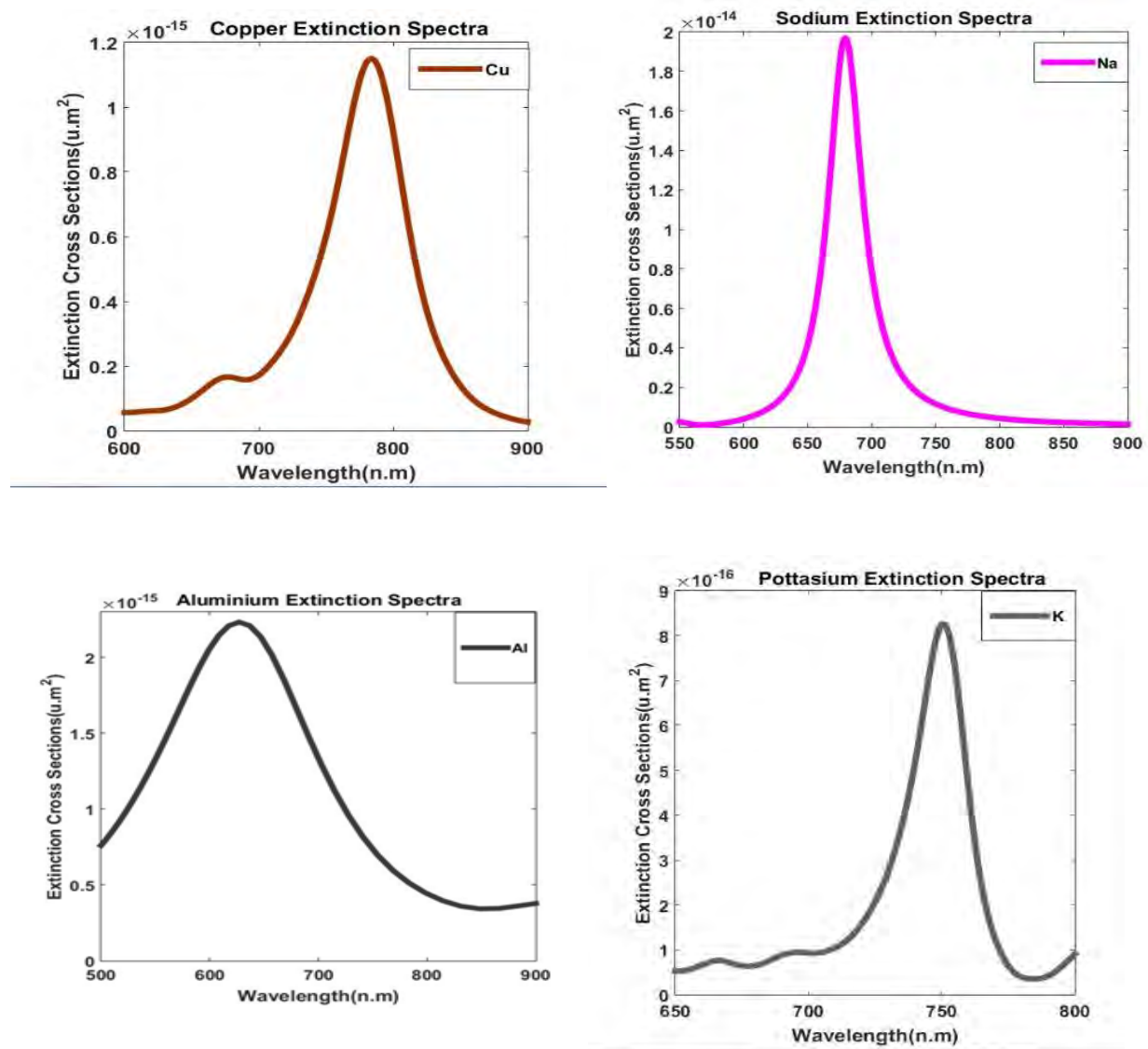
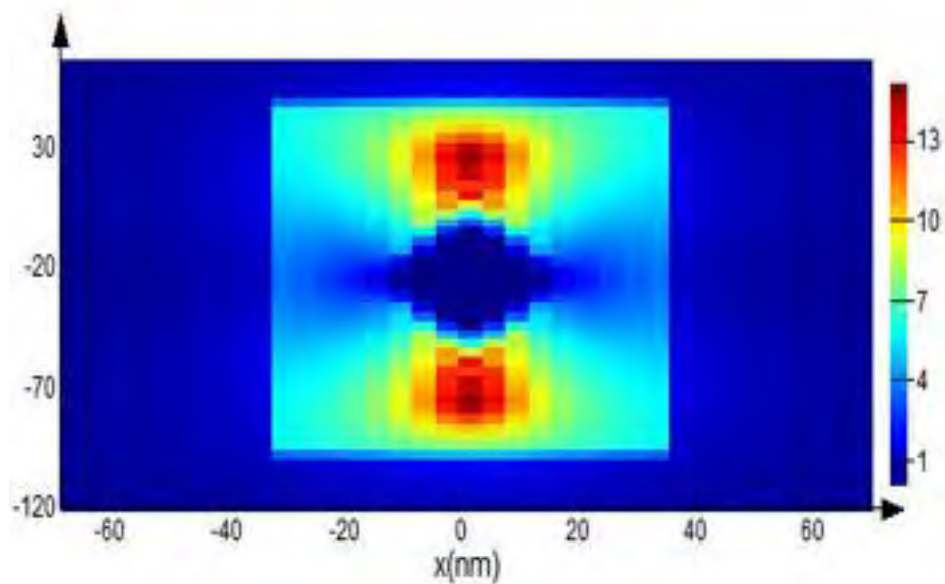


Figure 5.5 LSPR extinction spectra for a) Copper, b) Sodium, c) Aluminum d) Potassium



Here, we can see copper's LSPR peak is similar to gold. Copper is highly conductive and low of cost. Sodium and potassium have the sharpest peak as they are highly reactive and their losses in the visible spectrum are the lowest However, Aluminum is best for shorter wavelengths and it has huge losses in the visible and near infrared region [61].

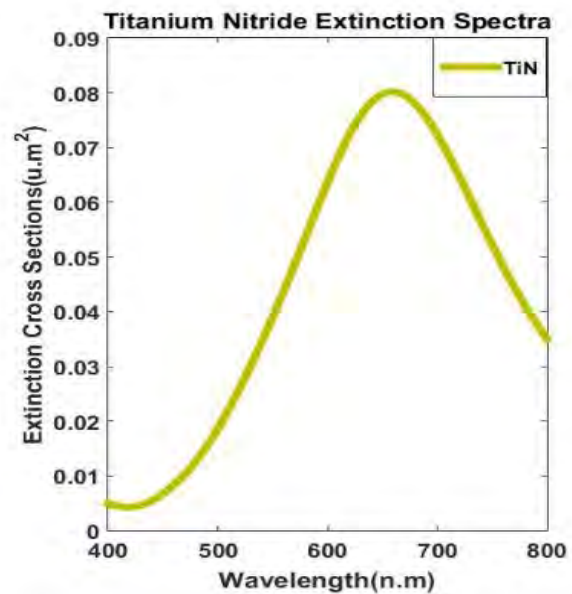
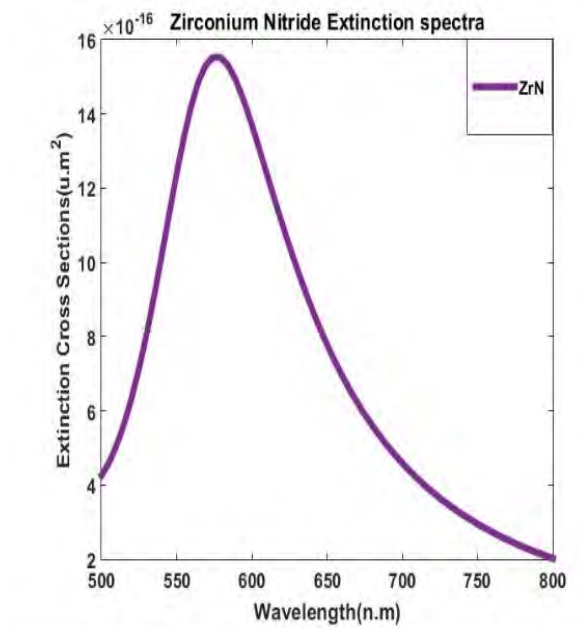
In analyzing the electric field enhancement profile, Sodium has the highest electric field enhancement of the three.

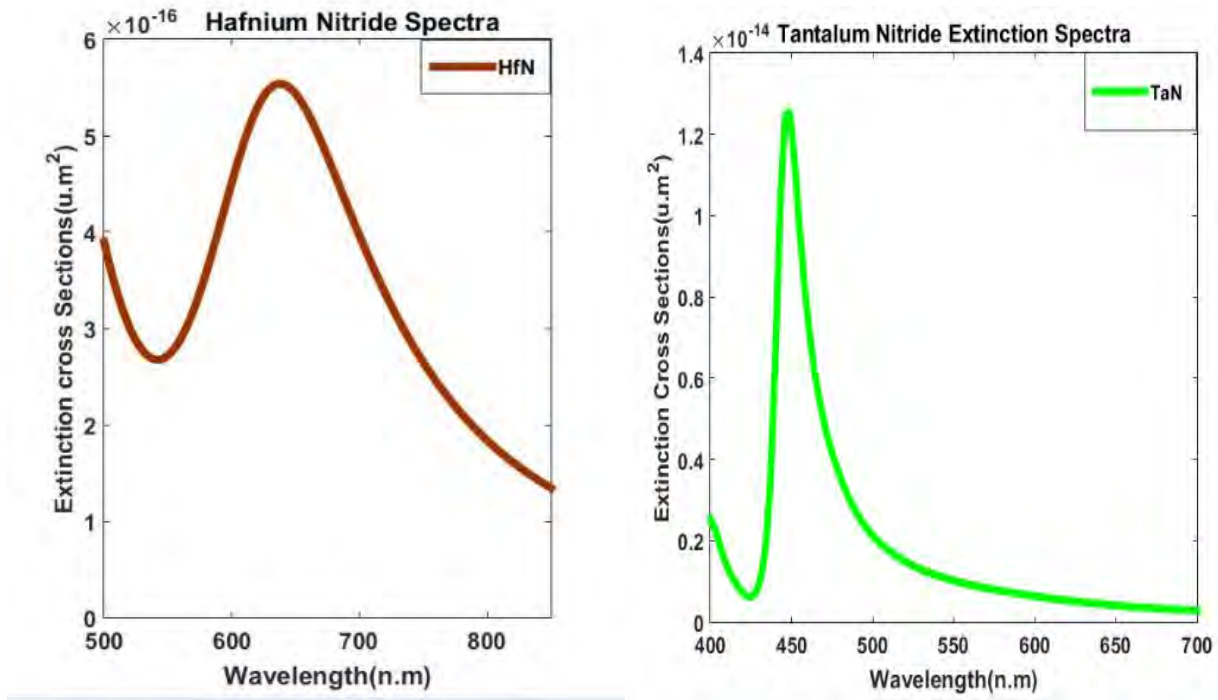


**Figure 5.5 Electric Field enhancement of Sodium**

## 5.5 Transitional Metal Nitrides:

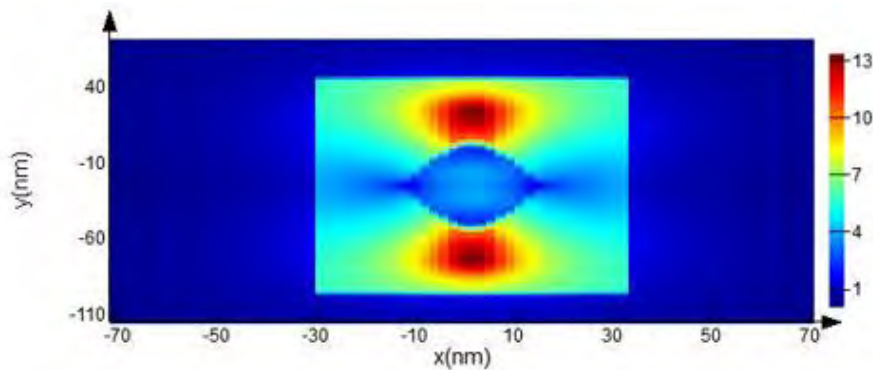
We have also modeled our Bipyramid as Transition metal nitrides such as ZrN, TiN, HfN, TaN . Analyzing the result we can see that these transition metal nitrides show LSPR peaks in the visible ranges. Zirconium Nitride has a LSPR peak at 570nm, Titanium Nitride has a LSPR peak at 664 nm, and Hafnium Nitride has a LSPR peak at 616nm. The LSPR peaks are shown in figure below.





**Figure 5.6 LSPR extinction peaks for a) Zirconium Nitride b) Titanium Nitride c) Hafnium Nitride c) Hafnium Nitride d) Tantalum Nitride**

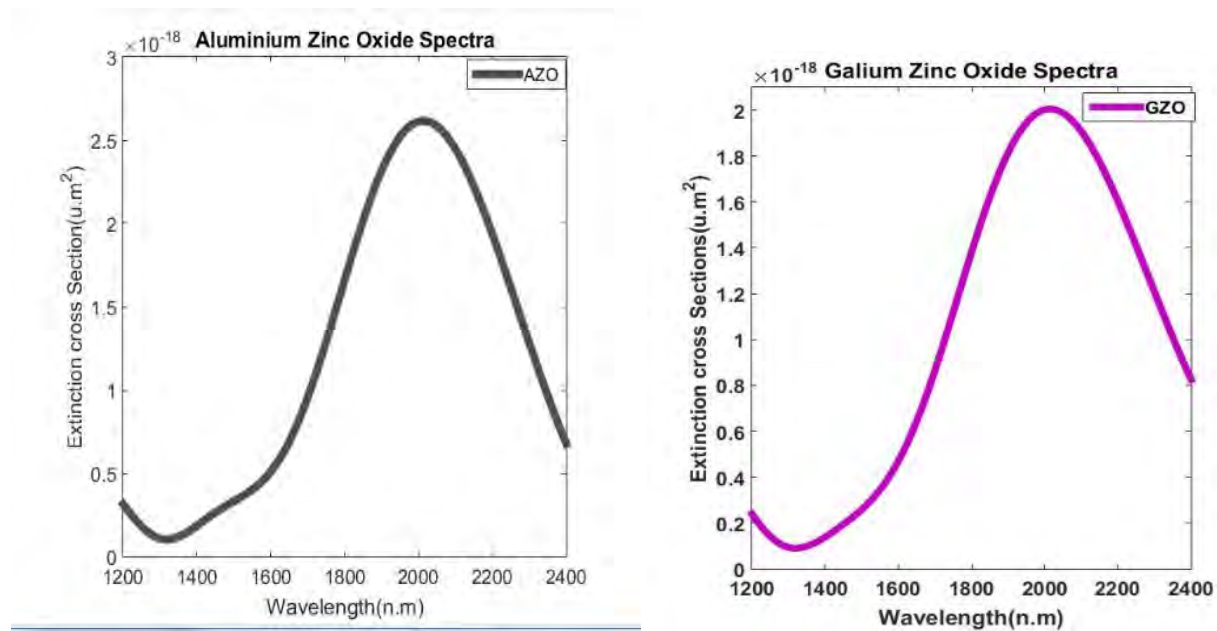
If we want the electric field enhancement we can see that titanium nitride has the highest intensity. The electric field enhancement profile is shown below



**Figure 5.7 Electric field enhancements for Titanium Nitride**

## 5.6 Transparent Conducting Oxides:

Transparent Conducting Oxides are oxide semiconductors which has large bandgap and they are transparent in the visible range. TCO's are used in display panels [60]. In our simulation we have used Aluminum Zinc Oxide, Gallium Zinc Oxide and Indium Tin Oxide as a material for our bipyramid model. We can see that AZO has a LSPR peak at 1890nm, GZO has a LSPR peak at 1880nm and ITO has a LSPR peak at 2000nm. As a result, we can say that TCO's are good plasmonic materials for infrared and near infrared ranges. The LSPR peaks of AZO, GZO, ITO are shown below.



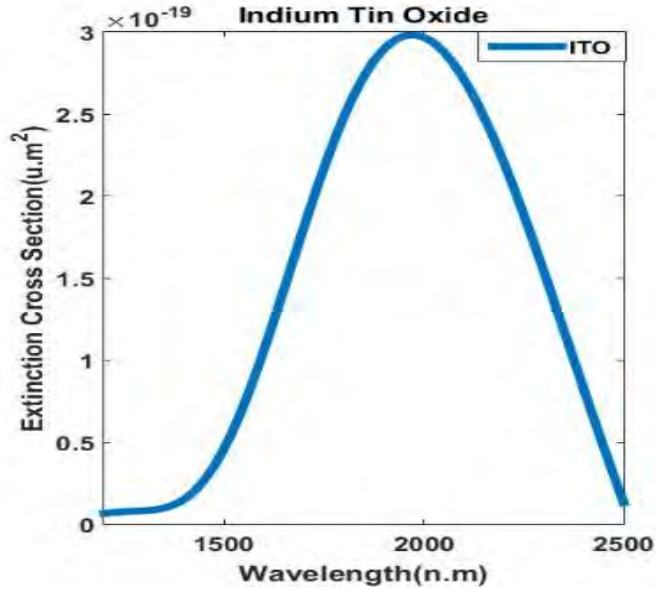


**Figure 5.8 LSPR extinction peaks for AZO, GZO, and ITO**

The electric enhancement field shows us that AZO has the highest intensity of the three. The electric field intensity for AZO is shown below.

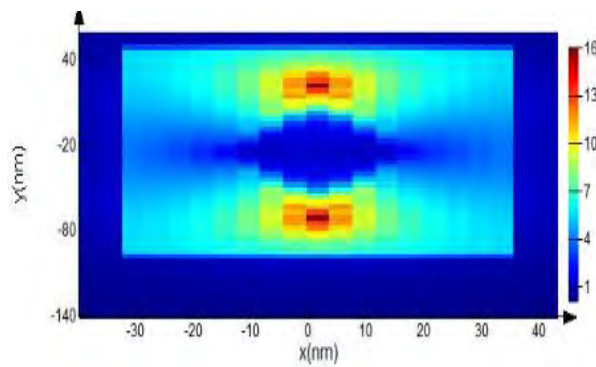


**Figure 5.9 Electric field enhancement for AZO**

## 5.7 Sensitivity Analysis and FOM:

In our simulation proteins which are bio markers for various diseases were used. We have used Lysozyme, Immunoglobulin, Human serum Albumin, Human Fibrinogen. The proposed was incident on TM polarized light the LSPR peak shifts determine a clear view of sensitivity of the system. In our simulation, we saw that for various proteins the peak shifted depending on the material. The sensitivity formula is given below

$$\text{Sensitivity} = d\lambda/dn$$

$d\lambda$  = The difference of wavelength from 2<sup>nd</sup> medium and 1<sup>st</sup> peak for the material

$dn$  = The difference between refractive index of 2<sup>nd</sup> medium and 1<sup>st</sup> medium

The main purpose of finding the sensitivity is to calculate the LSPR figure of merit for different materials. The Figure of Merit represents performance of a system relative to its alternatives. In our simulation we calculated the figure of merit for metals, transition metal nitrides and transparent conducting oxides. The table and figure below represents the different peaks for different protein refractive index and figure of merit for the used in the simulation.

Material	Extinction Cross sections(nm)					FOM
	H2O	Fb	IgG	HSA	LYS	
Au	800	804	807	815	825	4
Ag	906	914	923	940	944	6
Cu	788	794	798	809	812	2
Al	630	634	640	650	655	1.5
Na	662	665	668	674	684	3.5
K	761	763	767	770	789	1.7
ZrN	570	574	580	583	590	1.3
HfN	616	620	622	630	635	1
TaN	442	450	455	460	465	1.6
TiN	664	670	683	690	691	1.4
AZO	1890	1893	1897	1900	1905	2
GZO	1880	1885	1890	1895	1898	1.7
ITO	2000	2004	2006	2009	2012	1.2

Table 5.2 LSPR peaks for different materials and figure of merit calculation

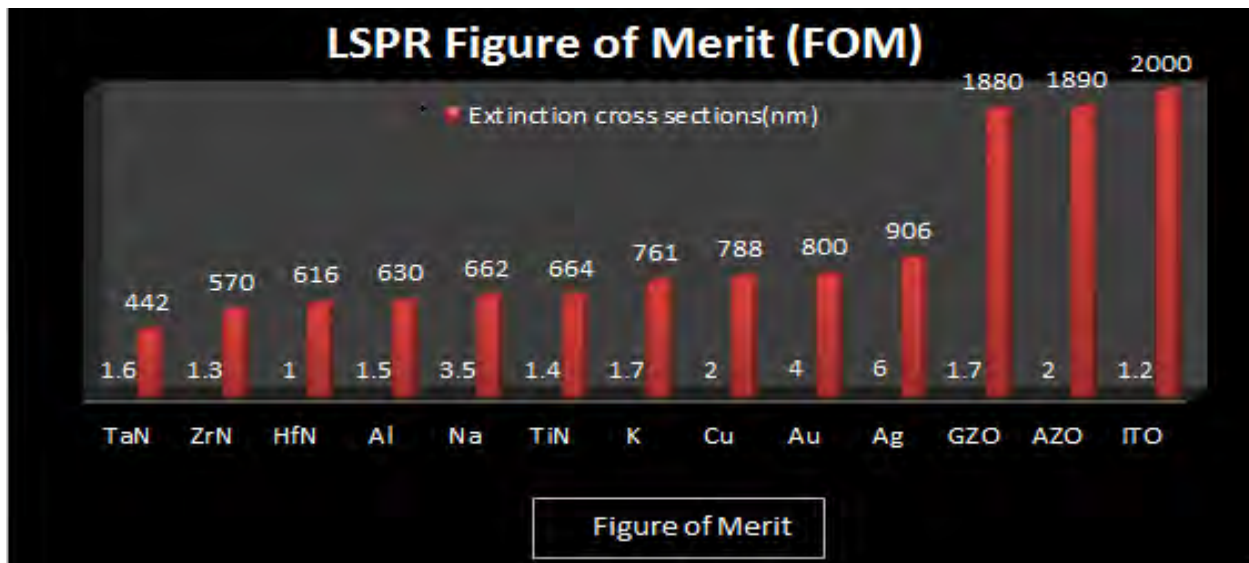


Figure 5.10 LSPR Figure of merit for different material

Observing our result we can see that for visible ranges metals and transition metals perform well. However TCO's perform well in the infrared region. Metals and Noble metals perform really well in the visible region however they are prone to have interband transition loss, degradation, oxidation and unstable. Metal Nitrides and TCO perform very well as they have higher bandgap energy and they suffer less loss.

## **5.8 Summary:**

Our main goal of the simulation was to investigate the molecular sensitivity and find the FOM of our proposed bi pyramid in terms of LSPR shifts. For this reason, we have used Different bio protein samples which are of significant importance in the medical sector. After our study, the nano bipyramid was found to be was found to be better than The conventional spherical structure. The accurate permittivity data for metals were found. However, the data for metal nitrides and TCO's were interpolated. The results would have been much better if we had the actual permittivity data for metal nitrides and TCO's.



## **Chapter 6**

### **Conclusion and Future works**

This thesis work mainly focuses LSPR characteristics in gold Bipyramid using metals transition metal nitrides and TCO's. Since gold and silver have already been considered two of the most preferable options for LSPR. However other materials such as alkali metals, transition metal nitrides and transparent conduction oxides are also viable for LSPR applications.

It is obvious from our findings that the bipyramid with different materials provide better results in presence of protein samples compared to the conventional gold structure. Therefore, the proposed structure can be more suitable for LSPR bio sensing applications.

Our next step will be to study Fano resonance properties of a single bipyramid structure which will add massive contribution to our work. In the future, we plan to experimentally verify the simulation results. The experimental verification will provide us to broaden the research opportunities of Bipyramid using various materials in bio sensing.

## Bibliography:

- [1] Chan, G. H., Zhao, J., Schatz, G. C., & Van Duyne, R. P. (2008). Localized surface plasmon resonance spectroscopy of triangular aluminum nanoparticles. *The Journal of Physical Chemistry C*, 112(36), 13958-13963.
- [2] Difference Between SPR and LSPR, <https://nicoyalife.com/technology/surface-plasmon-resonance/>
- [3] Chan, G. H., Zhao, J., Hicks, E. M., Schatz, G. C., & Van Duyne, R. P. (2007). Plasmonic properties of copper nanoparticles fabricated by nanosphere lithography. *Nano Letters*, 7(7), 1947-1952.
- [4] Abboud, J. E., Chong, X., Zhang, M., Zhang, Z., Jiang, N., Roy, S., & Gord, J. R. (2013). Photothermally activated motion and ignition using aluminum nanoparticles. *Applied Physics Letters*, 102(2), 023905.
- [5] Hammond, J. L., Bhalla, N., Rafiee, S. D., & Estrela, P. (2014). Localized surface plasmon resonance as a biosensing platform for developing countries. *Biosensors*, 4(2), 172-188.
- [6] Santra, S., Ghosh, P., & Biswas, A. (2014). Investigation of low loss heavily doped plasmonic semiconductors: Looking beyond lossy conventional noble metals. *International Journal of Emerging Technology and Advanced Engineering*, 4(4).
- [7] Maier, S. A. (2007). *Plasmonics: fundamentals and applications*. Springer Science & Business Media
- [8] illustration of the excitation of localized surface plasmon resonance, <https://www.intechopen.com/books/applications-of-molecular-spectroscopy-to->

[current-research-in-the-chemical-and-biological-sciences/enhanced-molecular-spectroscopy-via-localized-surface-plasmon-resonance](#)

[9] Jiang, H. (2011). Nanoplasmonic Sensors based on Periodic Arrays of Gold Nanoparticles.

[10] Lycurgus cup: a piece of Ancient Roman Nanotechnology, <http://www.amusingplanet.com/2016/12/lycurgus-cup-piece-of-ancient-roman.html>

[11] Mayer, K. M., & Hafner, J. H. (2011). Localized surface plasmon resonance sensors. *Chemical reviews*, 111(6), 3828-3857.

[12] Rivera, V. A. G., Ferri, F. A., & Marega Jr, E. (2012). Localized surface plasmon resonances: noble metal nanoparticle interaction with rare-earth ions. In *Plasmonics-Principles and Applications*. InTech.

[13] Schematics illustration of scattering and absorption spherical object, <https://www.etpl.sg/innovation-offerings/ready-to-sign-licenses/dsimie-overview-n-specifications>

[14] Grzelczak, M., Pérez-Juste, J., Mulvaney, P., & Liz-Marzán, L. M. (2008). Shape control in gold nanoparticle synthesis. *Chemical Society Reviews*, 37(9), 1783-1791.

[15] Daniel, M. C., & Astruc, D. (2004). Gold nanoparticles: assembly, supramolecular chemistry, quantum-size-related properties, and applications toward biology, catalysis, and nanotechnology. *Chemical reviews*, 104(1), 293-346.

[16] Lee, S. Y., Kim, S. H., Jang, S. G., Heo, C. J., Shim, J. W., & Yang, S. M. (2011). High-fidelity optofluidic on-chip sensors using well-defined gold nanowell crystals. *Analytical chemistry*, 83(23), 9174-9180.

- [17] Corbierre, M. K., Beerens, J., Beauvais, J., & Lennox, R. B. (2006). Uniform one-dimensional arrays of tunable gold nanoparticles with tunable interparticle distances. *Chemistry of materials*, *18*(11), 2628-2631.
- [18] Vedantam, P., Tzeng, T. R. J., Brown, A. K., Podila, R., Rao, A., & Staley, K. (2012). Binding of Escherichia coli to functionalized gold nanoparticles. *Plasmonics*, *7*(2), 301-308.
- [19] Rycenga, M., Cobley, C. M., Zeng, J., Li, W., Moran, C. H., Zhang, Q., ... & Xia, Y. (2011). Controlling the synthesis and assembly of silver nanostructures for plasmonic applications. *Chemical reviews*, *111*(6), 3669-3712.
- [20] Wang, H. H., Liu, C. Y., Wu, S. B., Liu, N. W., Peng, C. Y., Chan, T. H., ... & Wang, Y. L. (2006). Highly raman-enhancing substrates based on silver nanoparticle arrays with tunable sub-10 nm gaps. *Advanced Materials*, *18*(4), 491-495.
- [21] Feng, C., Xu, G., Liu, H., Lv, J., Zheng, Z., & Wu, Y. (2014). Glucose biosensors based on Ag nanoparticles modified TiO<sub>2</sub> nanotube arrays. *Journal of Solid State Electrochemistry*, *18*(1), 163-171.
- [22] Liu, C. H., Li, Z. P., Du, B. A., Duan, X. R., & Wang, Y. C. (2006). Silver nanoparticle-based ultrasensitive chemiluminescent detection of DNA hybridization and single-nucleotide polymorphisms. *Analytical chemistry*, *78*(11), 3738-3744.
- [23] Behrens, S., Wu, J., Habicht, W., & Unger, E. (2004). Silver nanoparticle and nanowire formation by microtubule templates. *Chemistry of materials*, *16*(16), 3085-3090.
- [24] Willets, K. A., & Van Duyne, R. P. (2007). Localized surface plasmon resonance spectroscopy and sensing. *Annu. Rev. Phys. Chem.*, *58*, 267-297.

- [25] El-Sayed, M. A. (2001). Some interesting properties of metals confined in time and nanometer space of different shapes. *Accounts of chemical research*, 34(4), 257-264.
- [26] Kelly, K. L., Coronado, E., Zhao, L. L., & Schatz, G. C. (2003). The optical properties of metal nanoparticles: the influence of size, shape, and dielectric environment.
- [27] Smitha, S. L., Gopchandran, K. G., Ravindran, T. R., & Prasad, V. S. (2011). Gold nanorods with finely tunable longitudinal surface plasmon resonance as SERS substrates. *Nanotechnology*, 22(26), 265705.
- [28] Mayer, K. M., & Hafner, J. H. (2011). Localized surface plasmon resonance sensors. *Chemical reviews*, 111(6), 3828-3857.
- [29] Szunerits, S., & Boukherroub, R. (2012). Sensing using localised surface plasmon resonance sensors. *Chemical Communications*, 48(72), 8999-9010.
- [30] Yanik, A. A., Cetin, A. E., Huang, M., Artar, A., Mousavi, S. H., Khanikaev, A., ... & Altug, H. (2011). Seeing protein monolayers with naked eye through plasmonic Fano resonances. *Proceedings of the National Academy of Sciences*, 108(29), 11784-11789.
- [31] Choi, I., Song, H. D., Lee, S., Yang, Y. I., Kang, T., & Yi, J. (2012). Core-satellites assembly of silver nanoparticles on a single gold nanoparticle via metal ion-mediated complex. *Journal of the American Chemical Society*, 134(29), 12083-12090.
- [32] Dreaden, E. C., Alkilany, A. M., Huang, X., Murphy, C. J., & El-Sayed, M. A. (2012). The golden age: gold nanoparticles for biomedicine. *Chemical Society Reviews*, 41(7), 2740-2779.
- [33] Huang, X., El-Sayed, I. H., Qian, W., & El-Sayed, M. A. (2006). Cancer cell imaging and photothermal therapy in the near-infrared region by using gold nanorods. *Journal of the American Chemical Society*, 128(6), 2115-2120.
- [34] Oulton, R. F., Sorger, V. J., Genov, D. A., Pile, D. F. P., & Zhang, X. (2008). A hybrid plasmonic waveguide for subwavelength confinement and long-range propagation. *nature photonics*, 2(8), 496-500.

- [35] Dragoman, M., & Dragoman, D. (2008). Plasmonics: Applications to nanoscale terahertz and optical devices. *Progress in Quantum Electronics*, 32(1), 1-41.
- [36] Kneipp, K., Wang, Y., Kneipp, H., Perelman, L. T., Itzkan, I., Dasari, R. R., & Feld, M. S. (1997). Single molecule detection using surface-enhanced Raman scattering (SERS). *Physical review letters*, 78(9), 1667.
- [37] Aslan, K., & Geddes, C. D. (2009). Directional surface plasmon coupled luminescence for analytical sensing applications: which metal, what wavelength, what observation angle?. *Analytical chemistry*, 81(16), 6913-6922.
- [38] Halas, N. J., Lal, S., Chang, W. S., Link, S., & Nordlander, P. (2011). Plasmons in strongly coupled metallic nanostructures. *Chem. Rev*, 111(6), 3913-3961.
- [39] Wu, J., Lu, X., Zhu, Q., Zhao, J., Shen, Q., Zhan, L., & Ni, W. (2014). Angle-resolved plasmonic properties of single gold nanorod dimers. *Nano-Micro Letters*, 6(4), 372-380.
- [40] Figure, Vörös, J. (2004). The density and refractive index of adsorbing protein layers. *Biophysical journal*, 87(1), 553-561.
- [41] **Biomarker**, <https://en.wikipedia.org/wiki/Biomarker>
- [42] Makarov, D. V., Loeb, S., Getzenberg, R. H., & Partin, A. W. (2009). Biomarkers for prostate cancer. *Annual review of medicine*, 60, 139-151.
- [43] **Lysozyme**, <https://en.wikipedia.org/wiki/Lysozyme>
- [44] **Lysozyme figure**, <https://en.wikipedia.org/wiki/Lysozyme>
- [45] Human serum Albumin, [https://en.wikipedia.org/wiki/Human\\_serum\\_albumin](https://en.wikipedia.org/wiki/Human_serum_albumin)
- [46] Human serum Albumin figure,  
[https://en.wikipedia.org/wiki/Human\\_serum\\_albumin](https://en.wikipedia.org/wiki/Human_serum_albumin)
- [47] Immunoglobulin, [https://en.wikipedia.org/wiki/Immunoglobulin\\_therapy](https://en.wikipedia.org/wiki/Immunoglobulin_therapy)
- [48] Immunoglobulin figure,  
[https://en.wikipedia.org/wiki/Immunoglobulin\\_therapy](https://en.wikipedia.org/wiki/Immunoglobulin_therapy)
- [49] Fibrinogen, <https://en.wikipedia.org/wiki/Fibrinogen>
- [50] Fibrinogen, <https://en.wikipedia.org/wiki/Fibrinogen>

- [51] FDTD, [https://en.wikipedia.org/wiki/Finite-difference\\_time-domain\\_method](https://en.wikipedia.org/wiki/Finite-difference_time-domain_method)
- [52] Jiang, H. (2011). Nanoplasmonic Sensors based on Periodic Arrays of Gold Nanoparticles.
- [53] Johnson, P. B., & Christy, R. W. (1972). Optical constants of the noble metals. *Physical review B*, 6(12), 4370.
- [54] Palik, E. D. (Ed.). (1998). *Handbook of optical constants of solids* (Vol. 3). Academic press.
- [55] Naik, G. V., Kim, J., & Boltasseva, A. (2011). Oxides and nitrides as alternative plasmonic materials in the optical range. *Optical Materials Express*, 1(6), 1090-1099.
- [56] Vörös, J. (2004). The density and refractive index of adsorbing protein layers. *Biophysical journal*, 87(1), 553-561.
- [57] Erickson, H. P. (2009). Size and shape of protein molecules at the nanometer level determined by sedimentation, gel filtration, and electron microscopy. *Biological procedures online*, 11(1), 32.
- [58] Solutions, F. D. T. D. (2003). Lumerical Solutions. Inc., <http://www.lumerical.com>.
- [59] Figure, Jiang, H. (2011). Nanoplasmonic Sensors based on Periodic Arrays of Gold
- [60] Naik, G. V., Shalaev, V. M., & Boltasseva, A. (2013). Alternative plasmonic materials: beyond gold and silver. *Advanced Materials*, 25(24), 3264-3294.
- [61] Chan, G. H., Zhao, J., Schatz, G. C., & Van Duyne, R. P. (2008). Localized surface plasmon resonance spectroscopy of triangular aluminum nanoparticles. *The Journal of Physical Chemistry C*, 112(36), 13958-13963.

